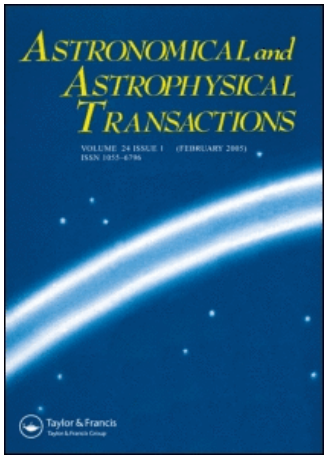

Astronomical & Astrophysical Transactions
The Journal of the Eurasian Astronomical Society
Publication details, including instructions for authors and subscription information:
http://www.informaworld.com/smpp/title~content=t713453505

Solar wind turbulence from radio occultation data

I. V. Chashei [a]; A. I. Efimov [b]; M. K. Bird [c]
[a] Lebedev Physical Institute, Moscow, Russia
[b] Institute of Radio Engineering & Electronics, Moscow, Russia
[c] Argelander-Institut für Astronomie, University of Bonn, Bonn, Germany

Online Publication Date: 01 December 2007
To cite this Article: Chashei, I. V., Efimov, A. I. and Bird, M. K. (2007) 'Solar wind turbulence from radio occultation data', Astronomical & Astrophysical Transactions, 26:6, 611 - 620
To link to this article: DOI: 10.1080/10556790701600515
URL: http://dx.doi.org/10.1080/10556790701600515

Astronomical and Astrophysical Transactions
Vol. 26, No. 6, December 2007, 611–620

Solar wind turbulence from radio occultation data

I. V. CHASHEI*†, A. I. EFIMOV‡ and M. K. BIRD§

†Lebedev Physical Institute, Moscow, Russia
‡Institute of Radio Engineering & Electronics, Moscow, Russia
§Argelander-Institut für Astronomie, University of Bonn, Bonn, Germany

(Received 19 July 2007)

Properties of plasma turbulence in the solar wind can be determined from radio frequency fluctuation measurements recorded during solar conjunctions. Noteworthy recent results were obtained from radio occultation experiments performed with the spacecraft *Galileo* in the interval 1994–2002 and *Ulysses* in 1991–1997. The power spectral index was calculated for the range of heliocentric distances $5\ R_S < R < 80\ R_S$ (R_S = solar radius) and the radial evolution of this parameter is discussed. *Galileo* data (at low solar latitudes) are compared with those recorded with *Ulysses* (high heliographic latitudes) during the solar activity minimum. Estimates of the turbulence outer scale are obtained using long *Galileo* frequency fluctuation records. It is found that the turbulence outer scale increases approximately linearly with increasing solar distance in the inner region of the developed solar wind. The observations are interpreted under the assumption that the density fluctuations are generated locally via nonlinear interactions of outwardly propagating Alfvén waves.

Keywords: Radio sounding; Solar wind; Solar wind turbulence

1. Introduction

Many years of solar wind plasma investigations by radio occultation [1–4] and *in situ* [5] methods have shown that turbulence is a permanent property of the interplanetary plasma at all heliocentric distances and heliolatitudes. Fluctuations of the electron density, magnetic field, velocity, etc. are characterized by spatial and temporal power spectra covering many decades in the wave number or temporal frequency domains, respectively. Turbulence evolution and its interaction with the background plasma is of great importance for solar wind physics, especially near the Sun where the plasma flow accelerates to supersonic and superalfvenic velocities. Unfortunately, the solar wind acceleration region is inaccessible for *in situ* methods, and only the radio occultation method gives information about the characteristics of plasma

*Corresponding author. Email: chashey@prao.ru

Astronomical and Astrophysical Transactions
ISSN 1055-6796 print/ISSN 1476-3540 online © 2007 Taylor & Francis
http://www.tandf.co.uk/journals
DOI: 10.1080/10556790701600515

turbulence. One modification of the radio occultation method is based on measurements of the radio frequency fluctuations. This observable has some advantages for investigation of solar wind density fluctuations compared with others (for instance, amplitude fluctuation measurements), because the large-scale regime of spatial density turbulence spectrum, where the turbulence energy density is greatest, produces most of the fluctuations of radio signal frequency.

Radio occultation experiments were carried out beginning from 1991 using coherent radio signals of the *Ulysses* spacecraft and in the period 1995–2003 with the *Galileo* spacecraft. A large volume of observational data was obtained during these experiments at heliocentric distances 5–80 R_S, which includes the outer region of plasma acceleration and the inner region of developed solar wind flow. The data were obtained at low heliolatitudes (*Galileo* and *Ulysses*) as well as at high latitudes (*Ulysses*). This paper briefly reviews main results on turbulence spectra and regimes deduced from the *Galileo* and *Ulysses* coronal radio sounding experiments for the period 1991–2002 with special interest on the period of solar activity minimum in 1995–1997.

2. Temporal spectrum of frequency fluctuations

In this section we consider the temporal frequency fluctuation spectrum of a radio wave passing through the plasma of the solar corona and received at Earth. The phase of a monochromatic wave with frequency ω_0 at time t is defined by the relation

$$\Phi(t) = \omega_0 t - \left(\frac{\omega_0}{c}\right) \int_0^L n(z,t)\mathrm{d}z, \tag{1}$$

where c is the velocity of light, $n(z,t)$ is the refraction index, the z-axis is directed along the line of sight, and L is the distance between the spacecraft and the receiver. The instantaneous wave frequency ω can be defined as

$$\omega = \frac{\mathrm{d}\Phi}{\mathrm{d}t}. \tag{2}$$

Assuming the well-known relation for the refraction index in a plasma

$$n(z,t) = \left(1 - \left(\frac{\omega_\mathrm{p}^2}{\omega_0^2}\right)\right) \tag{3}$$

where $\omega_\mathrm{p} = (4\pi \mathrm{Ne}^2/\mathrm{m})^{1/2}$ is the plasma frequency, $N(z,t)$ is the plasma density, e and m are the electronic charge and mass. For $\omega \gg \omega_\mathrm{p}$ one may use the above expressions to derive an equation for the frequency

$$\omega_0 \left(1 - \left(\frac{v_\mathrm{Z}}{c}\right)\right) + (\lambda r_\mathrm{e}) \frac{\mathrm{d}}{\mathrm{d}t} \left[\int_0^L N(z,t)\mathrm{d}z\right] \tag{4}$$

where $\lambda = 2\pi c/\omega_0$ is the wavelength, $r_\mathrm{e} = \mathrm{e}^2/(\mathrm{mc}^2)$ is the classical electron radius, and v_Z is the ray path projection of the spacecraft velocity relative to the observer. The value of v_Z is known from navigational data and the corresponding Doppler shift term can be subtracted from equation (4). The following expression may then be derived for the temporal power

spectrum $G_f(\nu)$ of random frequency fluctuations $\delta f(t)$, $2\pi\delta f(t) = \omega - \omega_0$

$$G(\nu) = A\nu^2 \int_0^L dz \int W_N(q_x = 2\pi\nu/V, q_y, q_z = 0) dq_y \tag{5}$$

where $\mathbf{q}$ is the turbulence spatial frequency (wave number), ν is the fluctuation frequency, $W_N(\mathbf{q})$ is the 3D power spectrum of plasma density turbulence, A is a constant, and V is the projection of the flow velocity of the density fluctuations perpendicular to the line of sight. The main contribution to the frequency modulation originates from a comparatively thin slab of turbulent plasma located near the ray path proximate point to the Sun. Thus, integration over z in equation (5) can be converted to a multiplication by the effective thickness of the slab ΔR_{eff}, which is of the order of the heliocentric distance of the ray path proximate point.

We assume further that the spatial 3D density turbulence spectrum $W_N(\mathbf{q})$ can be represented by a power law of the form

$$W_N(\mathbf{q}) = C_N(r)(q^2 + q_0^2)^{-p/2} \tag{6}$$

where C is the structure constant, q_0 is the inverse turbulence outer scale, $q_0 = L_0^{-1}$, and p is the power exponent in the inertial spectral range. The influence of the turbulence inner scale is neglected here because its associated fluctuation frequency is much larger than the Nyquist frequency under the real experimental conditions. In this case the power spectrum of frequency fluctuations $G_f(\nu)$ in the frequency range $2\pi\nu > 2\pi\nu_{max} \approx q_0 V$ is also a power law [6]

$$G(\nu) = B\nu^{-\alpha} \tag{7}$$

where B = constant, and the power exponent $\alpha = p - 3$. For the power spectrum (6) with a turbulence outer scale, one expects to find a spectral turnover at lower frequencies $2\pi\nu < 2\pi\nu_{max}$. Due to the factor ν^2 in equation (5), this low-frequency turnover is more pronounced in the frequency fluctuation power spectra than in the phase fluctuation spectra. The maximum spectral density $G(\nu_{max})$ is proportional [7] to the variance σ_N^2 and bulk flow velocity V of the density fluctuations.

3. Observations

Coronal sounding experiments were conducted using the radio signals of the spacecraft *Ulysses* and *Galileo* during their solar conjunctions. *Ulysses* used phase coherent dual-frequency downlinks at the carrier frequencies 2.293 GHz (S-band) and 8.408 GHz (X-band). *Galileo* was constrained to single frequency 2.295 GHz (S-band), but this signal was generated on board by an ultra-stable oscillator (USO), resulting in a sensitivity nearly equivalent to the *Ulysses* radio science experiment.

The radio signals were recorded at the three 70 m tracking stations Canberra (DSS 43), Madrid (DSS 63) and Goldstone (DSS 14) of the NASA Deep Space Network (DSN). The signal frequency was recorded at a nominal sampling rate of 1 s^{-1}. Doppler residual time series were calculated by subtracting a slowly-varying component from the raw data to compensate for the spacecraft motion relative to the observer. Temporal power spectra were calculated using a standard FFT algorithm for all observational intervals with a duration longer than 4×4096 samples. Spectral indices α were determined for the spectral ranges where the power spectra

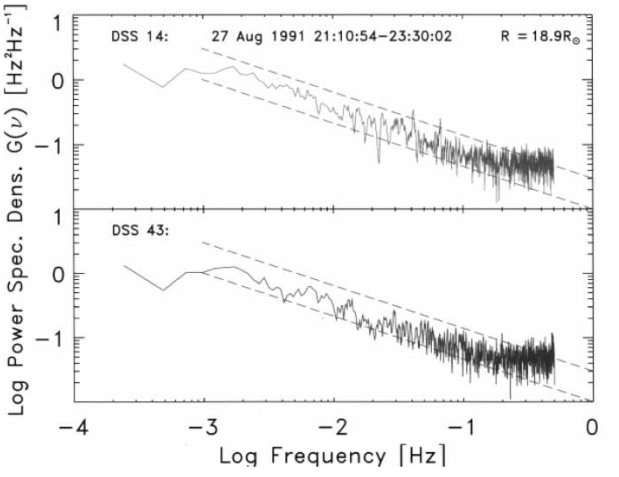

Figure 1. Examples of the frequency fluctuations power law spectra.

can be represented as power law. Some typical frequency fluctuation spectra are illustrated in figure 1.

Simultaneous Doppler recordings from two widely-spaced receivers, which provide the capability for estimating the bulk velocity of the inhomogeneous medium, occur during the frequent observation overlap intervals between DSN stations. For these overlap periods, the speed of the inhomogeneities was found as the ratio of the calculated two-station ray path radial separation to the time lag of maximum frequency cross-correlation between the two stations. The typical duration of the overlap intervals is about 2 hours, and the typical ray path radial separation for these occasions is several thousand kilometres. An example of a frequency fluctuation cross-correlation function is presented in figure 2.

Some observation *Galileo* sessions have very long duration, up to several tens of hours. On these occasions, the low-frequency turnover could be detected in the frequency fluctuation power spectra. An example power spectrum with low-frequency turnover is presented in figure 3.

Estimates of the turbulence outer scale were obtained [7] from the relation $q_0 V \sim \nu_{\max}$ using the known values of the frequency of maximum spectral power $\nu_{\max}$ and the velocity of the inhomogeneities V.

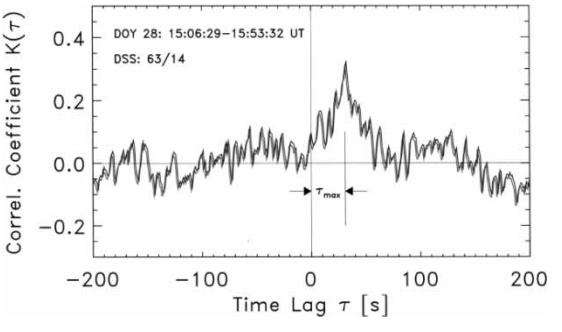

Figure 2. Examples of the frequency fluctuations cross-correlation function.

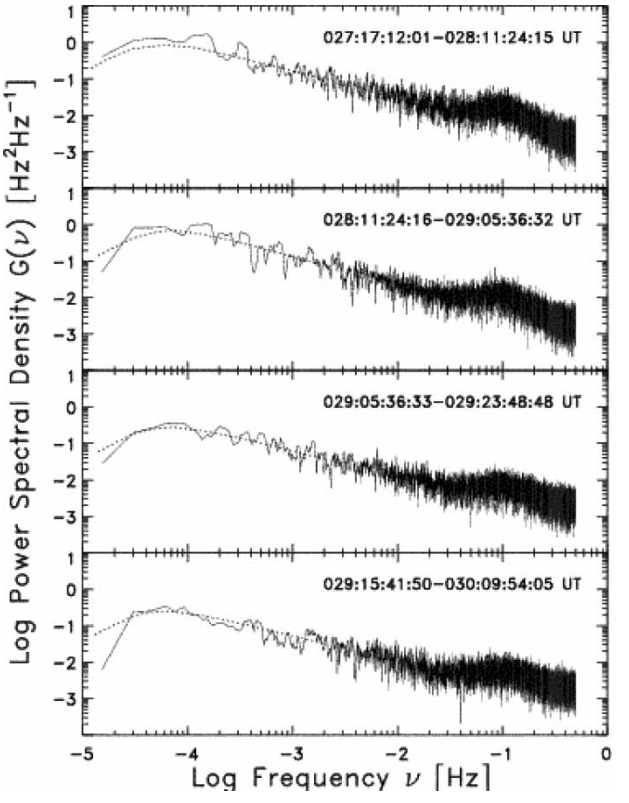

Figure 3. Examples of the power spectra with low frequency turn over.

4. Radial evolution of power law turbulence spectra

Typical frequency fluctuation power spectra assume the form of a power law over the central range of temporal frequencies. These spectra have a smooth local maximum at some frequency $\nu_{\max}$ and a power law spectral interval for $\nu > \nu_{\max}$ that extends up to frequencies where the measured fluctuation power drops to the noise level. Parameters available for study of their radial evolution are the frequency of spectral maximum $\nu_{\max}$, the maximum spectral density $G(\nu_{\max})$, and the power law index α at $\nu > \nu_{\max}$. The radial dependence of the power law index α for low heliolatitudes ($\varphi < 10°$), derived from *Galileo* and *Ulysses* data during the years 1991–1997, is presented in figure 4.

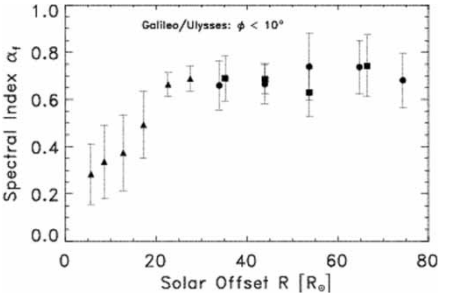

Figure 4. Radial dependence of the power spectral index from the *Galileo* and *Ulysses* data.

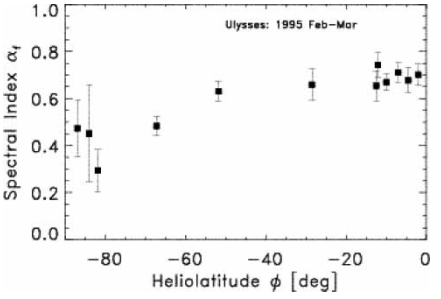

Figure 5. Power spectral index from the *Ulysses* data.

Considering results from both spacecraft to increase the data volume, average values of α and its standard deviation are presented for 10 R_S bins in the range 30–80 R_S, 5 R_S bins in the range 10–30 R_S, and 2.5 R_S bins in the range 5–10 R_S. Circles and squares denote measurements on the west and east solar limbs, respectively. Data averages below 30 R_S (triangles) were taken from both solar limbs. The power exponent α clearly increases with heliocentric distance from values $\alpha \approx 0.2$ up to $\alpha \approx 0.6 - 0.7$ at $R > 20$ R_S and remains approximately constant for $R > 20$ R_S. The observed value of α at $R > 20$ R_S is consistent with the expected value $\alpha = 2/3$ for Kolmogorov turbulence spectra. The 3D power index of the density turbulence power spectra $p = \alpha + 3$ must follow the same radial dependence. A similar trend was found earlier [8] from spectral analysis of Viking radio signal phase fluctuations.

The *Ulysses* data of 1995 are well suited for investigating the heliolatitude dependence of the spectral index α. As shown in figure 5, $\alpha \approx 2/3$ in the range of heliolatitude $-50° < \varphi < 0°$, but has a tendency to decrease when the line of sight approaches the south polar region. These results agree with the spectral changes found in phase fluctuation spectra [9].

The data of figure 5 most likely reflect a real heliolatitude dependence for the spectral index α. The variation in solar offset distance during this measurement interval was rather moderate (22 $R_S < R < 32$ R_S). Whereas the spectral index $\alpha \approx 2/3$ within this distance range at low heliolatitudes (figure 4), figure 5 shows that the spectral index of the frequency fluctuation spectrum is substantially less than $2/3$ at heliolatitudes $|\varphi| > 65°$. We thus conclude that the transition from flat to steeper turbulence spectra occurs at greater heliocentric distances in high latitude regions (figure 5) than at low latitudes (figure 4).

Seven coronal sounding campaigns were carried out during the active lifetime of the *Galileo* spacecraft in the years 1994–2002 at different phases of solar activity cycle #23. No significant correlation could be found between the measured statistical parameters of frequency fluctuations and the level of solar activity. The radial profile of the power exponent α, the radial falloff of RMS density fluctuations σ_N and the absolute turbulence level are all approximately the same at different phases of the solar activity cycle. Only relatively low heliolatitudes were sounded by the *Galileo* spacecraft.

5. Fractional density fluctuations in the inner solar wind

We now use the frequency fluctuation data to derive the fractional density fluctuations over the range of heliocentric distances from 7 R_S up to 31 R_S. The RMS values of density fluctuations in the solar wind σ_N were calculated from the measured values of maximum spectral density $G(\nu_{max})$, the power exponent α, and the velocity of the inhomogeneities V estimated from overlapping two-station records. The estimates of σ_N from *Galileo* are valid for the period of

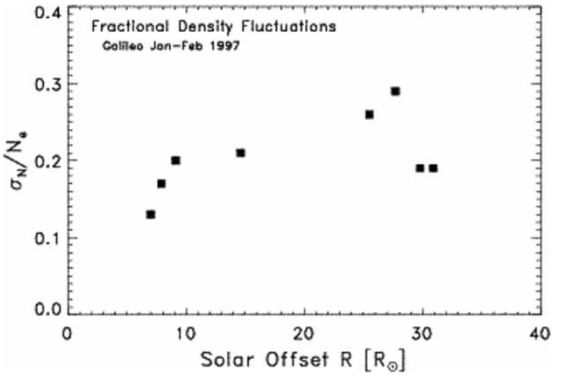

Figure 6. Radial dependence of the fractional density fluctuations.

low solar activity in January–February 1997. Typical values of σ_N range from 10^2 to 10^3 cm^{-3}. Results from Viking ranging measurements [10], which are applicable to the epoch of solar minimum, were used for computing the mean electron density N_e. The radial dependence of the fractional density fluctuations σ_N/N_e, valid here for the slow solar wind, is shown in figure 6.

The fractional density fluctuations are typically of the order of 0.1–0.3 at low heliolatitutes and low solar activity levels. These estimates are in good agreement with the results [11] from a study of *Ulysses* dual-frequency ranging data, which are applicable to temporal frequencies in the range 6×10^{-5} Hz $< \nu < 8 \times 10^{-4}$ Hz.

The data of figure 6 display a slight tendency for an increase in the fractional density fluctuations σ_N/N_e with heliocentric distance. The same trend was found for fast solar wind streams [11]. The data presented in figure 6 thus extend this conclusion to the slow solar wind.

6. Turbulence outer scale

Estimates of the turbulence outer scale were deduced from the measured frequencies of maximum spectral density ν_{max} using *Galileo* data when long duration records and two-station velocity measurements were available simultaneously [7]. The radial dependence of the turbulence outer scale $L_0 \approx V/\nu_{max}$ is presented in figure 7 for the period near solar activity minimum in the years 1995/1996.

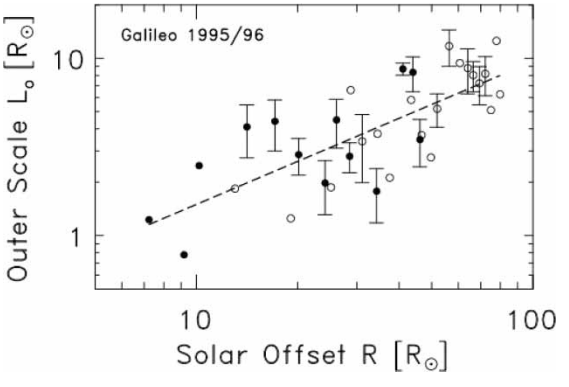

Figure 7. Radial dependence of the turbulence outer scale.

Figure 7 clearly shows that the turbulence outer scale increases with increasing heliocentric distance. The radial dependence of the turbulence outer scale can be approximated by a power law function $L_0 = a(\mathrm{R}/\mathrm{R_S})^m$ with the fitting parameters a ≈ 0.24 R_S and $m \approx 0.8$ over the range of heliocentric distances 8 $\mathrm{R_S}$ < R < 80 $\mathrm{R_S}$, *i.e.*, the region of developed solar wind flow at constant speed.

7. Discussion and comparison with the theoretical model

A reasonable interpretation of the observational results presented above is provided by a model [12] that considers the solar wind turbulence to be driven by a random ensemble of interacting Alfvén and magnetosonic waves. The turbulence energy source is provided by low frequency Alfvén waves propagating outward from the coronal base. The magnetosonic waves responsible for the density fluctuations are generated locally by nonlinear wave–wave interactions. The magnetic field is strong in the solar wind acceleration region (R < 20 $\mathrm{R_S}$) so that the Alfvén speed is larger than the speed of sound. The turbulence here is weak and the density fluctuations are dominated by slow magnetosonic waves. Accordingly, power spectra for the magnetic field and density fluctuations are comparatively flat, with a 3D power-law index $p = 3.0$ (*i.e.*, corresponding to $\alpha = 0$, consistent with the frequency fluctuation measurements). Such spectra are formed as a result of the nonlinear conversion of Alfvén quanta to lower frequencies by conservation of their total number. It is very important that these power spectra are noncascading, *i.e.*, the flux of turbulent energy to the small-scale spectral range is absent. The same turbulence power spectra in the solar wind acceleration region were deduced for the magnetic field fluctuations inferred from *Helios* spacecraft Faraday rotation measurements [13]. Moreover, recent analysis of visible angular sizes of microwave subsecond solar radio bursts have shown that flicker-type spectra ($p = 3$) also occur in the inner solar corona [14].

The fractional level of turbulence increases with heliocentric distance because the energy density of the Alfvén waves decreases more slowly than the energy density (magnetic plus thermal) of the ambient plasma. Moreover, the ratio of the speed of sound to the Alfvén speed also increases. The combination of these two effects results in an increase of the fractional level of fast magnetosonic waves, thereby enhancing the cascading process and the corresponding transition to developed turbulence characterized by steeper spectra of the types Kolmogorov ($p = 11/3, \alpha = 2/3$) or Kraichnan ($p = 7/2, \alpha = 1/2$). This transition, as well as the increase in fractional turbulence level, is observed in the radio sounding measurements. The transition zone is located at R ≈ 20 $\mathrm{R_S}$, thereby coinciding with the radial evolution from the acceleration region to the region of fully developed solar wind. The more distant transition for the fast solar wind can be explained by the stronger magnetic field above the coronal holes and, as a consequence, the lower values of fractional turbulence level and ratio of sound to Alfvén speed.

The fact that there is no observable difference between the years near solar activity minimum and those near solar maximum implies that the properties of MHD-turbulence in the low-latitude slow solar wind are, on average, independent of the phase of solar activity cycle. It is known that changes in coronal magnetic field topology, which are presumably responsible for cyclic modulation of the global solar wind structure, are strongly pronounced only at high heliolatitudes. Whereas a bimodal global structure with fast solar wind at high latitudes and slow solar wind at low latitudes is observed for the solar activity minimum, nearly isotropic slow solar wind emanates from the Sun at solar maximum. Our study thus provides additional evidence that the turbulence regime of the solar wind is controlled by coronal magnetic fields. Similar to the cyclically varying global solar wind structure, one can expect strong cyclic changes in the turbulence at high heliolatitudes.

The radial dependence of the turbulence outer scale in the developed solar wind was compared with the theoretical trend [7] expected in a model for which the outer scale separates spectral regions $q < q_0$, dominated by linear MHD wave propagation effects, and $q > q_0$, where nonlinear interactions are of main importance. The following types of nonlinear interactions have been considered: strong interactions (Kolmogorov turbulence), three-wave decay interactions (Iroshnikov–Kraichnan turbulence) and four-wave interactions. The best agreement with the observed radial dependence of the outer scale was found for the three-wave interaction model [7].

The above considerations show that important conclusions on the physics of the turbulent inner solar wind may be drawn from radio sounding data. An analysis of radio occultation results in combination with *in situ* measurements would be particularly beneficial. Turbulence temporal spectra measured by *in situ* and radio-sounding methods correspond to 1D and 2D spatial power spectra, respectively. A comparison of spectra derived from *in situ* density fluctuations and radio phase (or frequency) fluctuations thus provide valuable information about the anisotropy of density inhomogeneities. Furthermore, conclusions concerning the physical origin of turbulence can be inferred from 1D/2D turbulence spectra and fractional fluctuation levels of the density or any other fluctuating plasma parameter with the same statistical characteristics such as magnetic field, bulk velocity, etc. In particular, such comparisons should provide a better understanding of the role of Alfvén waves in the local generation of density fluctuations. In this context, it should be noted that evidence for local nonlinear generation of magnetosonic waves by Alfvén waves has been found [15] from a comparison of the fractional levels of magnetic field and density fluctuations measured *in situ* in the solar wind near 1 AU.

8. Conclusions

The following conclusions may be drawn from the above results and discussion.

- As a rule, spatial turbulence power spectra in the inner solar wind take the form of a power law over a wide range of fluctuation scales.
- The regimes of solar wind turbulence in the acceleration region and in the developed solar wind are distinctly different: power spectra are comparatively flat for $R < 20\ R_S$; and become steeper for $R > 20\ R_S$.
- During the period of minimum solar activity the change of turbulence regime occurs at greater heliocentric distances for (fast) high-latitude solar wind than for (slow) low-latitude solar wind.
- The fractional density fluctuations tend to increase with increasing heliocentric distance inside $25\ R_S$, but more data are needed to confirm this preliminary conclusion.
- No changes in the turbulence regime were found over the solar activity cycle at low heliolatitudes.
- The turbulence outer scale increases approximately linearly with increasing heliocentric distance over the range $10\ R_S < R < 80\ R_S$.
- The observations are in a good qualitative agreement with a theoretical model based on the assumption of local generation of density fluctuations by Alfvén waves propagating from the coronal base.

Acknowledgements

The present work was supported by the Program "Plasma processes in the solar system" of the Russian Academy of Sciences. This paper presents results of research partly funded by the

Deutsche Forschungsgemeinschaft (DFG) under a cooperative program between the DFG and the Russian Foundation of Basic Research (RFBR). The authors wish to express their gratitude for the continued support of the Galileo Project, the Multi-Mission Radio Science Team and the NASA Deep Space Network.

References

[1] O.I. Yakovlev, A.I. Efimov, V.M. Razmanov and V.K. Strykov, Sov. Astron. Zhourn. **24** 454 (1980).
[2] M.K. Bird, Space Sci. Rev. **33** 99 (1982).
[3] M.K. Bird and P. Edenhofer, *Physics of the Inner Heliosphere*, Heidelberg, Springer-Verlag, p. 13 (1990).
[4] R. Wohlmuth, D. Plettemeier, P. Edenhofer *et al.*, Space Sci. Rev. **97** 9 (2001).
[5] C.Y. Tu, and E. Marsch, 1995, Space Sci. Rev. **73** 1 (1995).
[6] I.V. Chashei, A.I. Efimov, L.N. Samoznaev, D. Plettemeier and M.K. Bird, Adv. Space Res. **36** 1454 (2005).
[7] A.I. Efimov, I.V. Chashei, L.N. Samoznaev *et al.*, Astron. Rep. **46** 640 (2002).
[8] R. Woo and J.W. Armstrong, J. Geophys. Res. **84** 7288 (1979).
[9] M. Pätzold, J. Karl and M.K. Bird, Astron. Astrophys. **316** 449 (1996).
[10] D.O. Muhleman and J.D. Anderson, Astrophys. J. **247** 1093 (1981).
[11] R. Woo, J.W. Armstrong, M.K. Bird and M. Pätzold, Geophys. Res. Lett. **22** 329 (1995).
[12] I.V. Chashei and V.I. Shishov, Sov. Astron. Zhourn. **27** 346 (1983).
[13] I.V. Chashei, A.I. Efimov, L.N. Samoznaev, M.K. Bird and M. Pätzold, Adv. Space Res. **25** 1973 (2000).
[14] I.V. Chashei, V.I. Shishov and A.T. Altyntsev, 2006, Astron. Rep. **83** 282 (2006).
[15] S.R. Spangler and L.G. Spitler, Physics Plasmas **11** 1969 (2004).